High-performance Tunable Multichannel Absorbers Couple with Graphene-based Grating and Dual-Tamm Plasmonic Structures

Jinlei Hu
Jiangnan University
Zhengda Hu
Jiangnan University
Jicheng Wang (jcwang@jiangnan.edu.cn)
Jiangnan University https://orcid.org/0000-0003-2814-2302
Aliaksei Balmakou
Francisk Skorina Gomel State University: Gomel'skij gosudarstvennyj universitet imeni Franciska Skoriny
Sergei Khakhomov
Francisk Skorina Gomel State University: Gomel'skij gosudarstvennyj universitet imeni Franciska Skoriny
Igor Semchenko
Francisk Skorina Gomel State University: Gomel'skij gosudarstvennyj universitet imeni Franciska Skoriny

Research Article

Keywords: Tamm plasmon polariton , transfer matrix theory , photonic crystal , multichannel absorption filter

DOI: https://doi.org/10.21203/rs.3.rs-463336/v1

High-performance tunable multichannel absorbers couple with graphene-based grating and dual-Tamm plasmonic structures

Jinlei Hu,[a] Zhengda Hu,[a] Jicheng Wang(✉),[a,b] Aliaksei Balmakou,[c] Sergei Khakhomov,[c] and Igor Semchenko,[c]

[a]*School of Science, Jiangsu Provincial Research Center of Light Industrial Optoelectronic Engineering and Technology, Jiangnan University, Wuxi 214122, China*
[b]*State Key Laboratory of Applied Optics, Changchun Institute of Optics, Fine Mechanics and Physics, Chinese Academy of Sciences, Changchun 130033, China*
[c]*Departments of Optics, Francisk Skorina Gomel State University, Gomel 246019, Belarus*

✉ Corresponding authors. E-mail: jcwang@jiangnan.edu.cn

Abstract We present a hybrid Tamm system targeting the tunable multichannel absorber. The proposed optical absorber is analyzed and investigated by using the transfer matrix method (TMM). The numerical and theoretical studies show that the four perfect absorption peaks are generated by two types of resonant modes excited in the structure, which can be reasonably explained by the guide-mode resonance (GMR) and optical Tamm state (OTS). More importantly, the strong interaction between the two modes gives rise to mode hybridization by adjusting the grating period. Furthermore, the active modulation of the GMR-based peak can be manipulated discretely by tuning the polarization angle or continuously by changing the chemical potential of graphene. The presented optical absorption filter will meet high level of effectiveness in developing high-performance optoelectronic devices.

Keywords Tamm plasmon polariton • transfer matrix theory • photonic crystal • multichannel absorption filter

Introduction

In recent years, there has been an increased interest in a special type of surface electromagnetic states called the optical Tamm states (OTSs) because of their potential applications in narrow-bandwidth multichannel absorbers and thermal emission devices [1-3]. These states are analogous to the Tamm states in condensed matter physics. The first proposed OTS is excited between two photonic crystals (PhCs) [4]. Subsequently, the OTS generated near the interface between metal and photonic crystal is proposed, which is also called Tamm plasmon polariton (TPP) [5,6]. The PhC is a special structure produced by the periodic stacking of high refractive index materials [7] and low refractive index materials. And the common Bragg reflector (BR) is a simple one-dimensional PhC in optics [5, 13].The two materials in the BR need to have a good light transmission in the considered waveband and the specific lattice structure periodicity [8,9]. Compared with traditional surface states such as surface plasmon polarization (SPP) [10-12], TPP modes could be excited with either TE or TM polarization [13,14] without requiring for a specific incident angle [15-17].

The plasmonic reaction of graphene and the applications of Tamm structure have attracted widespread attention [18-22]. Plasmonic reaction, which occurs in many semiconductors and metals, is ubiquitous, high-frequency, collective density oscillations of an electron liquid [19]. Graphene, an attractive, atomically thin carbon material that can replace metals, has shown plasmonic reaction in the infrared region, featuring greatly enhanced electric field and ultra-fast optical tunability [19,20]. Surface plasmons (SPs) in graphene are electromagnetic waves that propagate along the surface of the graphene due to the infrared light-induced oscillation of surface charges, which can effectively enhance optical absorption [20-22]. In order to better improve the light absorption performance of the graphene monolayer, a simple method of guided mode resonance (GMR) can be introduced to maintain SPs [23-25]. It is difficult to realize TPP in practice because the photonic local field of the Tamm plasmon is near the interface between the metal film and the photonic crystal, that is, inside the Tamm structure. There are currently three research techniques to make the idea workable: adjusting the structure of the photonic crystal, changing the structure of the metal layer, or using the coupling of the Tamm structure with other structures to distribute the photonic local field in an appropriate position. Lundt et al. utilized organic materials to connect metal thin films and photonic crystals, then embedded single-layer tungsten diselenide films [26] and single-layer molybdenum diselenide films [27] into the connection materials. The organic material has a refractive index similar to that of the low refractive index material in the photonic crystal. Mischok et al. investigated a metal-organic-metal microcavity structure to replace the metal layer in the Tamm structure, and realized the regulation of the Tamm plasmon by changing the organic layer [28]. Das et al. numerically determined two reverse Tamm structures to add materials to be detected in the metal cavity, facilitating the design of a temperature sensor [29] and a refractive index sensor [30].

In this paper, we propose to achieve high-performance tunable multichannel absorption filters based on the grating layer and metal-photonic crystal heterostructure-metal (M-PCH-M). The GMR and TPP resonance can be excited simultaneously at near-infrared frequencies. The simulation results show that the three high efficiency TPP peaks can be maintained by adjusting the thickness of thin silver films and the top layer thickness in the M-PCH-M. Furthermore, the strong coupling between the two modes gives rise to mode hybridization. Transfer matrix theory (TMT) have been employed to explain the strong coupling phenomenon. To investigate the optical properties in this hybrid structure, simulations are achieved by using the finite element method. In addition, the modulation of GMR-based absorption can be actively controlled by adjusting the polarization angle or chemical potential of graphene. The proposed optical multichannel absorption filter has potential applications in modulators, solar cells, sensors, thermal radiation.

Structure and theory

In Fig. 1(a), we demonstrate a part of the hybrid Tamm structure, in which the M-PCH-M structure is deposited on a ZnO film and a thick silver layer substrate. The x and y directions of the structure are infinitely extended. In the COMSOL simulation, in order to simplify the calculation, we only simulate the modeling of the x-z section and the y direction is infinitely wide by default. Periodic boundary conditions are set on both sides of the structure in the x direction, and perfectly matched layers are added up and down to absorb the outgoing light. By using periodic boundary

conditions, the simulation of complex structures can be simplified into periodic elements to improve convergence. Meeting the phase matching condition [35,36] in Eq. (11), a plane wave of TM polarization (i.e., electric field has no component in the y direction) or TE polarization (i.e., the electric field has a component in the y direction) is injected onto the structure at an angle of θ to excite the TPP mode at the interface between the PhC and thin silver layer. The thickness of ZnO layer in the structure is 12 nm, and the upper and lower layers in the M-PCH-M structure are thin sliver films, with the thickness of t_m=27 nm. The silver substrate with a thickness much larger than the penetration depth of the incident radiation is added under the structure to block all transmission. The dielectric constant of silver can be characterized by the Drude model [31]:

$$\varepsilon_r = \varepsilon_\infty - \frac{\omega_p^2}{\omega^2 + i\omega\gamma} - \frac{\Delta \times \Omega^2}{(\omega^2 - \Omega^2) + i\Gamma}, \quad (1)$$

where ε_∞=2.4064 is the dielectric constant when the frequency of the incident light ω tends to infinity, γ=2π×4.8×10^{12} Hz is the collision frequency, ω_p=2π×2214.6×10^{12} Hz is the plasmon frequency, Δ=1.6604 is the weight coefficient of Lorentz item, Ω=2π×620.7×10^{12} Hz is the strength of Lorentz harmonic oscillator, Γ=2π×1330.1×10^{12} Hz is the spectral width of vibration.

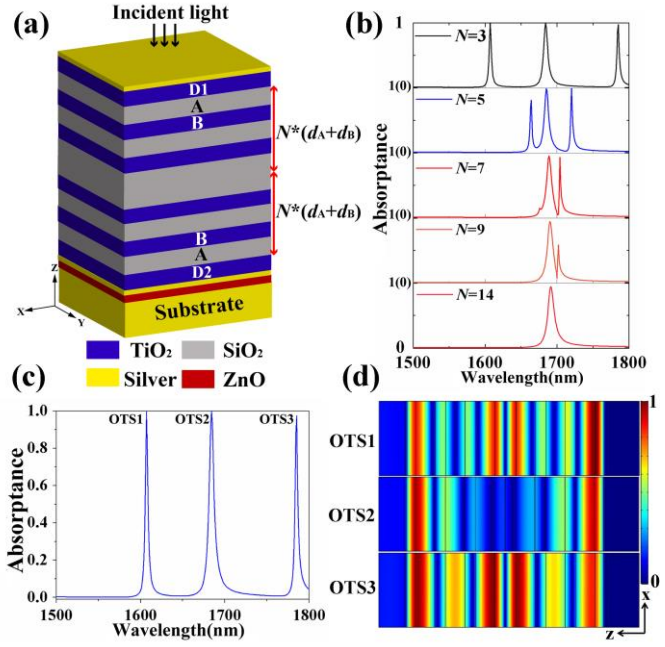

Fig. 1 (a) Schematic diagram of the structure composed of upper silver film/PCH/lower silver film/ZnO/silver substrate; (b) The two side peaks can be eliminated by increasing the number of layers N of the dual PhCs; (c) The three perfect absorption peaks were realized for the depicted structure when N=3; (d) The electric field distributions for the three peaks corresponding to TPP modes: OTS1, OTS2, OTS3.

In the simulated structure, the PhC is composed of alternating layers of silicon dioxide (SiO_2) and titanium dioxide (TiO_2). As a one-dimensional photonic crystal, the BR is a reflector used in a waveguide. When light passes through different media, it will be reflected at the interface, and the reflectivity will be related to the refractive index between the media [5, 13]. Here the refractive indices of SiO_2 and TiO_2 are n_A=1.45 and n_B=2.6, respectively. The conditions of Bragg incident light are met by selecting the thickness of the SiO_2 and TiO_2 layers: $d_A=\lambda_M/4n_A$ and $d_B=\lambda_M/4n_B$, where λ_M is the central resonant wavelength of BR. The number of periodic layers of PhCs are both N. In order to effectively excite the OTSs, a material with a higher refractive index should be incorporated as the top layer. The relevant material of the top layer D1 and lower layer D2 is determined to be TiO_2, with their thickness to be optimized at D=136 nm.

With the increase of the number of periodic layers N of the dual PhCs, the Tamm absorption peaks of the structure gradually changes as shown in Fig. 1(b). When the number N of the dual PhCs increases from 3 to 14 pairs continuously, the side TPP peaks gradually move inside just to finally merge into a single peak. Fig. 1(c) is the absorptance spectrum of the designed structure being excited by the TE polarization when incident normally when N=3. It can be seen from the Fig. 3(c) that the electric field enhancement with wavelengths of 1607 nm and 1785 nm are mainly distributed at the interface of dual PhCs and M-PhC. And the electric field enhancement with wavelength of 1684 nm is mainly concentrated on the two interfaces of M-PhC and PhC-M.

The transmission characteristics of the M-PCH-M part of the structure can be analyzed by the TMM:

$$E_{out} = ME_{in}, \quad (2)$$

where E_{out} and E_{in} are the electric field of output light and incident light respectively, and M is the transfer matrix of light in the structure, which can be expressed as follows:

$$M = \begin{bmatrix} M_{11} M_{12} \\ M_{21} M_{22} \end{bmatrix} = m_{Ag} m_{D1} (m_A m_B)^N (m_B m_A)^N m_{D2} m_{Ag}, \quad (3)$$

where, m_{Ag}, m_{D1}, m_A, m_B, m_{D2} represent the transmission matrix

of light through each layer, and N are the number of periodic layers of the two photonic crystals.

The TMM of incident light in each layer can be expressed as:

$$m_i = \begin{bmatrix} \cos\delta_i & -ip_i^{-1}\sin\delta_i \\ -ip_i\sin\delta_i & \cos\delta_i \end{bmatrix}. \quad (4)$$

In formula 4, $\delta_i=(2\pi/\lambda)n_i d_i\cos\theta_i$, where $n_i d_i$ is the optical thickness of the corresponding layer, θ_i is the angle between the light in the dielectric layer and the normal direction of the interface, and λ is the wavelength of incident light. When the incident light is incident with TM or TE polarization, the corresponding p_i has the following formulas:

$$p_i = \sqrt{\varepsilon_0\mu_0}\,n_i/\cos\theta_i, \quad (5)$$

$$p_i = \sqrt{\varepsilon_0/\mu_0}\,n_i\cos\theta_i, \quad (6)$$

where $i=m_{Ag}$, m_D, m_{SiO2} or m_{TiO2}, then ε_0 is the vacuum dielectric constant and μ_0 is the permeability of vacuum.

The transmission coefficien t and reflection coefficient r of light can be expressed as

$$t = \left|\frac{2p_0}{(M_{11}+M_{12}p_t)p_0+(M_{21}+M_{22}p_t)}\right|, \quad (7)$$

$$r = \left|\frac{(M_{11}+M_{12}p_t)p_0-(M_{21}+M_{22}p_t)}{(M_{11}+M_{12}p_t)p_0+(M_{21}+M_{22}p_t)}\right|, \quad (8)$$

where the subscript '0' and 't' represent the incident and transmission space respectively. Therefore, the reflectance R and transmittance T of the light absorber can be determined in the following ways:

$$R = |r|^2, \quad (9)$$

$$T = \frac{p_t}{p_0}|t|^2. \quad (10)$$

Therefore, the absorptivity of the optical absorber can be calculated by A=1-R-T. As the bottom part of the designed absorber is containing a metal ground plane represented by a sliver substrate, the transmittance T is basically reduced to zero.

Simulations and Results

To explore the key features of the designed structure that are responsible for its effectiveness, we calculated the relationship between the absorption and several important structural parameters. One of them, D, is the thickness of the high refractive index TiO_2 layers D1 nd D2 located on the top of the upper and lower photonic crystals. It can be seen in Fig. 2(a) that with decreasing the thickness D, the TPP peaks have undergone relatively obvious blue shifts with substantially different slope ratios. As the absorptance of the resonance peak is relatively high when D=136nm, the thickness of the corresponding layer of the basic model structure is set to 136nm. Fig. 2(b) shows that as t_m, the thickness of the silver film increases, the positions of the three resonance peaks remain basically unchanged. t_m=27 nm has been chosen as the default value when carrying out a variation analysis and topological optimization of the designing absorber.

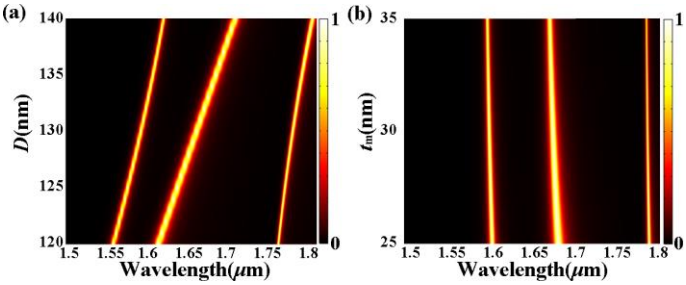

Fig. 2 Spectral diagrams determine the absorptance peak positioning depending on: (a) the thickness D and (b) t_m.

Fig. 3(a) shows a hybrid Tamm structure of the absorber with a graphene-based grating added onto the basic structure. The structure has two different types of resonance modes to achieve multiple absorption peaks, and the coupling effect of GMR and TPP modes on the improvement of absorption has been studied. In addition to enhancing the absorption of GMR peaks, the graphene monolayer, sandwiched between the grating and a dielectric layer of SiO_2 can increase tunability of the structure. Here we set the grating constant (also called the grating period) P=1.15 μm, the thickness and width of the opaque part are h=0.4 μm and W=0.25 μm respectively, and the dielectric matching layer thickness d=1 μm. Graphene monolayer thickness determined at t_g=0.34 nm with its dielectric permittivity $\varepsilon_g=1+i\sigma_g/(\omega\varepsilon_0 t_g)$, where σ_g is the surface conductivity of graphene and ε_0 is the vacuum dielectric constant, ω is the angular frequency of the incident wave. The conductivity is highly dependent on the chemical potential μ_c, which is determined at 0.3eV in this work taking into account the data [32,33]. The upper spectrum in Fig. 3(b) shows the absorptance when the resonance mode is excited by the TM

polarization. For this structure, the graphene-based grating has little effect on the propagating light, which is almost equal to completely transmitting to the surface of the thin silver flim of the Tamm structure. The spectrum shows three distinct TPP peaks with wavelengths of 1607 nm, 1684 nm and 1785 nm, corresponding to three optical Tamm states, similar to those depicted in Fig. 1(c). The lower spectrum in Fig. 3(b) resulted from the TE polarization excitation revealing a GMR peak at the wavelength of 1524 nm while keeping the same three OTSs, corresponding to the same three TPP resonance peaks. So this structure can be used for multi-channel absorption filter devices, which can perfectly absorb incident light of four wavelengths at the same time to achieve a filtering effect. Fig. 3(c) illustrates a Fabry Pérot (F-P) cavity resonance model, which has been proposed to understand the localization of the TPP resonances [34]. Because the one-dimensional PhC structure is relatively simple, it can be regarded as BR [13]. The excitation condition of the TPP mode generated at the interface of the BR and metal can be expressed as [5]:

$$r_M r_{BR} \exp(2i\delta) = 1, \tag{11}$$

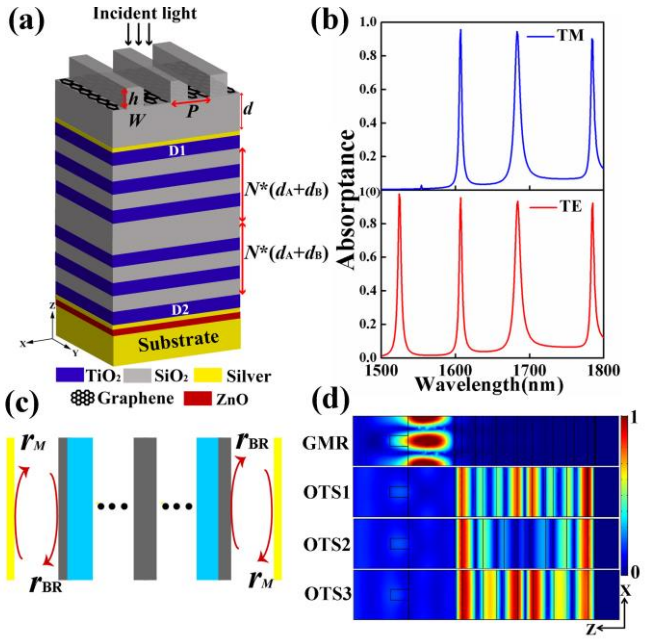

Fig. 3 (a) Three-dimensional schema of the multichannel absorption filter; (b) Absorption spectra when incident with TM and TE polarization respectively; (c) shows two identical cavities, both wrapped by silver films and BRs; (d) Electric field magnitude for the GMR and for three TPP modes when incident with TE polarization.

where δ is the phase change between the interfaces, r_M represents the reflection coefficient for the wave incident on the silver layer from the BR, which can be obtained by the Fresnel formula, r_{BR} is the reflection coefficient of the wave incident on the BR from the silver layer, which can be calculated by the transfer matrix method (TMM).

The resonance wavelength of the guided mode should meet the phase matching condition [35,36]:

$$k_{GMR} - k_0 \sin\theta = m\frac{2\pi}{P}, \tag{12}$$

where $k_{GMR}=k_0 \cdot n_{eff}$ is the wave vector of the guided mode, n_{eff} represents the effective refractive index of the guided mode, m is the diffraction order, and $k_0=2\pi/\lambda$ is the wave number where λ is the incident wavelength. In particular, when $\theta=0$ and $m=1$, the above formula can be reduced to $\lambda_0=n_{eff} \cdot P$. To better understand the GMR and TPP effect, the electric field distribution at the resonance is necessary to look at Fig. 3(d), from which it becomes clear that the GMR mainly occurs in the SiO_2 isolation layer, forming a typical standing wave profile. In other words, if the incident wave couples well with the leakage guided mode, GMR will occur. At the same time, it has been explained above that the TPP mode can be excited at the interface between the metal and the photonic crystal structure and between photonic crystals.

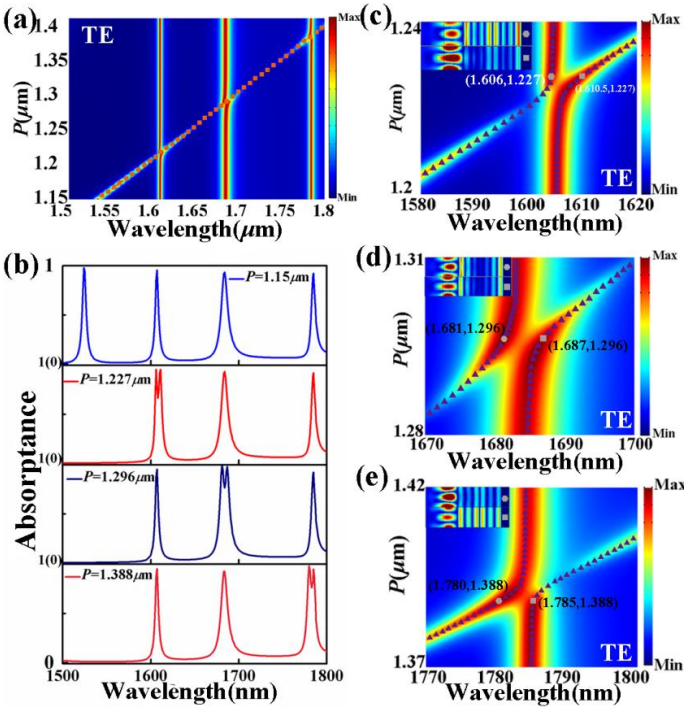

Fig. 4 Evolution of absorption spectra of (a) the hybridized

Tamm structure with the grating period length P, where the red square indicate the GMR; (b) Absorption spectrum at specific P; (c), (d), (e) are enlarged views of the absorption spectra at the three resonance coupling locationsare. The insets show the enhanced electric field resonance of GMR and TPP at the locations marked by hexagons and squares.

As shown in Fig. 4, changing the grating period length P will allow investigating the coupling effect between the GMR and TPP resonance depending on the wavelength and the polarization type (TE polarization). In Fig. 4(a), the analytical results obtained using Eq. (12) and results of numerical simulations are combined. As the P increases, the wavelength capable of exciting the GMR increases too, and at the corresponding P, the GMR couples with three TPP resonances. According to classic the two oscillator models, the frequency of the resonant mixed mode can be determined by [37-40]

$$f_{\pm} = \frac{f_{GMR} + f_{TPP}}{2} \pm \frac{\sqrt{(f_{GMR} - f_{TPP})^2 + \Omega^2}}{2}. \quad (13)$$

Here, $f_{\pm}$ is the resonance frequency of the hybrid modes, f_{GMR} and f_{TPP} represent the frequency of the GMR and the TPP resonance, and Ω is the interaction frequency between the two resonances. The dispersion relationship between GMR and TPP resonance can be calculated. The overlap between the two resonances occurs when varying the P. However, the two resonances will not impose exactly, but are separated by a small energy gap, exhibiting typical mode hybridization. The dotted curve marked by the purple triangles in the Fig. 4(c-e) is theoretically confirms the fact.

Fig. 4(b) shows the absorptance spectrum at variable P, indicating that the GMR is capable of being hybridized with any of the three TPP resonances. It can be seen that the mode hybridization slightly increases the width of the absorption peak and the absorptance, which can be applied to the adjustment of the absorption filter in the narrow band. The split of curves visible in Fig. 4(c-e) and associated with the resonance hybridization is called the Rabi split of the vacuum field [41-43]. It is necessary to note that the GMR and TPP resonances for all three cases are well described by theoretical approximation derived from Eq. 12 (dotted lines).

The GMR effectiveness is very sensitive to any variations with the chemical potential μ_c of the graphene grating, while the TPP resonances are irrelevant to the variations. In particular, when considering the 1524 nm resonance, the peak absorptance drops from 97.57% to 32.86% when μ_c increases from 0.4 eV to 0.42 eV, as shown in Fig. 5(a-b). The polarization angle of the incident linearly polarized radiation is capable of influencing the GMR absorptance spectrum as it is shown in Fig. 5(c,d), while the symmetry of the PhCs guarantees the independence of the TPP resonances on the polarization angle.

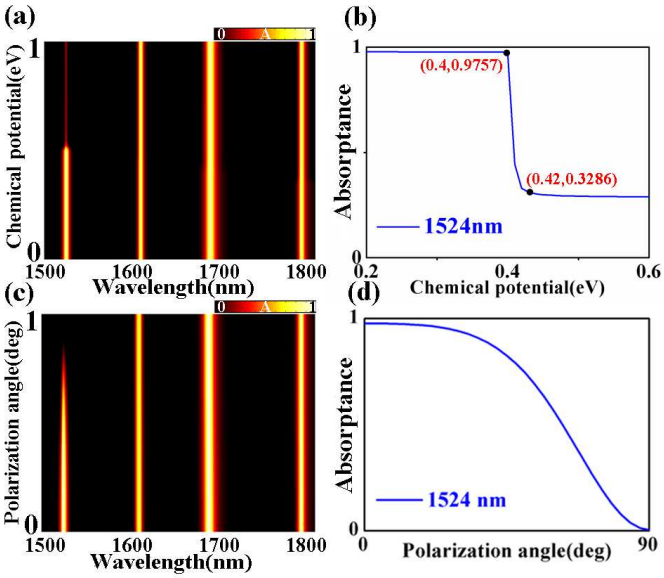

Fig.5 (a) Spectral diagram representing the dependence of the absorption as a function of the wavelength and the chemical potential of graphene under TE polarization. (b) The dependence of absorptance versus chemical potential at 1524 nm. (c) Spectral diagram representing the dependence of the absorptance as a function of the wavelength and the polarization angle at normal incidence. (d) The dependence of absorptance versus chemical potential at 1524 nm.

Conclusions

In general, the reason for the design of this structure is to explore the optical properties of the graphene-based grating combined with the double tam structure. Through simulation research, the structure can realize the tunable multi-channel absorption effect and can be applied to the near-infrared optical filter. Using the TMM, CMT, and numerical simulations (COMSOL multiphysics), the results reveal that four remarkable absorption peaks are generated due to GMR and TPP. The grating period length variation facilitates the GMR relocation along the spectra and superimposing with the TPP resonances, resulting in obvious mode hybridization. The

sliver thin film thicknesses used in the design of the absorber (M-PHC-M) can be varied without limiting the absorber's functionality. The positioning of the absorption peaks can be tuned by adjusting the thicknesses of the absorber's layers. In additional, the absorption filters can be used for selective polarization filtering of linearly-polarized radiation, the throughput of which can be controled by adjusting the chemical potential of graphene. The type of absorber can be potentially used as a part of optical devices such as sensors, modulators, switches, filters and polarizers, etc.

Fundings

This work was supported in part by the National Natural Science Foundation of China (11811530052), the Intergovernmental Science and Technology Regular Meeting Exchange Project of Ministry of Science and Technology of China (CB02-20), the China Postdoctoral Science Foundation (2017M611693, 2018T110440), the Open Fund of State Key Laboratory of Applied Optics (SKLAO2020001A04), the Grant of State Committee for Science and Technology of Belarus (F19KITG-017), and the Training Programs of Innovation and Entrepreneurship for Undergraduates of Jiangsu Province and China (201910295051Z, 201910295067).

Conflicts of interest

The authors declare no conflict of interest.

Availability of data and material

The data and material that support the findings of this study are available from the corresponding author upon reasonable request.

Code availability

The code that support the findings of this study are available from the corresponding author upon reasonable request.

Authors' contributions

Conceptualization, L.H. and J.W.; methodology, L.H. and J.W..; software, Z.B. and Z.D.H.; validation, A.B. and Z.B.; formal analysis, Z.B, Z.D.H., J.W.; writing--original draft preparation, Z.B., J.W., A.B.; writing--review and editing, A.B., S.K., and I.S.; visualization, Z.B.; supervision, J.W.; project administration, J.W., S.K.; funding acquisition, J.W. All authors have read and agreed to the published version of the manuscript.

Consent to participate

The authors declare that they have no conflicts of interest.

Consent for Publication

The authors grant the Publisher the sole and exclusive license of the full copyright in the Contribution, which license the Publisher hereby accepts. Consequently, the Publisher shall have the exclusive right throughout the world to publish and sell the Contribution in all languages, in whole or in part, including, without limitation, any abridgement and substantial part thereof, in book form and in any other form including, without limitation, mechanical, digital, electronic and visual reproduction, electronic storage and retrieval systems, including internet and intranet delivery and all other forms of electronic publication now known or hereinafter invented.

Reference

1. Gao H, Li P, Yang S (2020) Tunable multichannel optical absorber based on coupling effects of optical Tamm states in metal-photonic crystal heterostructure-metal structure. Opt. Commun. 457: 124688.

2. Goto T, Dorofeenko A V, Merzlikin A M, Baryshev A V, Vinogradov A P , Inoue M, Lisyansky A A, Granovsky A B (2008) Optical Tamm States in One-Dimensional Magnetophotonic Structures. Phys. Rev. Lett. 101: 113902.

3. Wang X Y, Wang J C, Liu D D, Hu Z D, Zhang F (2018) Perfect absorption of molybdenum disulfide-based modified Tamm plasmonic structures. Applied Physics Express, 11(6): 062601.

4. Kavokin A V, Shelykh I A, Malpuech G (2005) Lossless interface modes at the boundary between two periodic dielectric structures. Phys. Rev. B 72(23): 3102.

5. Kaliteevski M, Iorsh I, Brand S, Abram R A, Chamberlain J M, Kavokin A V, Shelykh I A (2007) Tamm plasmon-polaritons: Possible electromagnetic states at the interface of a metal and a dielectric Bragg mirror. Physical review. B, Condensed Matter And Materials Physics, 76(16): p.165415.1-165415.5.

6. Sasin M E, Seisyan R P, Kalitteevski M A, Brand S, Abram R A, Chamberlain J M, Egorov A Y, Vasil Ev A P, Mikhrin V S, Kavokin A V (2008) Tamm plasmon polaritons: Slow and spatially compact light. Appl. Phys. Lett. 92: 251112.

7. Vasily V, Klimov, Andrey A, Pavlov, Ilya V, Treshin, Ilya (2017) Fano resonances in a photonic crystal covered with a perforated gold film and its application to bio-sensing. Journal of Physics D Applied Physics.

8. Jiang X, Wang T, Zhong Q, Yan R, Huang X (2020), Ultrabroadband light absorption based on photonic topological transitions in hyperbolic metamaterials. Opt. Express 28: 705.

9. Tsurimaki Y, Tong J K, Boriskin V N, Semenov A, Ayzatsky M I, Machekhin Y P, Chen G, Boriskina S V (2017) Topological Engineering of Interfacial Optical Tamm States for Highly Sensitive Near-Singular-Phase Optical Detection. Acs. Photonics 5: 929-938.

10. Pianelli A, Kowerdziej R, Dudek M, Sielezin K, Olifierczuk M, Parka J (2020) Graphene-based hyperbolic metamaterial as a switchable reflection modulator. Opt. Express 28: 6708.

11. Shao H, Chen C, Wang J, Pan L, Sang T (2017) Metalenses based on the non-parallel double-slit arrays. Journal of physics. D, Applied physics 50: 384001.

12. Yang L, Wang J, Yang L, Hu Z D, Wu X, Zheng G (2018) Characteristics of multiple Fano resonances in waveguide-coupled surface plasmon resonance sensors based on waveguide theory. Scientific Reports, 8: 2560.

13. Brand S, Kaliteevski M A, Abram R A (2009) Optical Tamm states above the bulk plasma frequency at a Bragg stack/metal interface. Physical Review B Condensed Matter 79(8): 85416-85416.

14. Senanayake P, Hung C H, Shapiro J, Lin A, Liang B, Williams B S, Huffaker D L (2011) surface Plasmon-Enhanced Nanopillar Photodetectors. Nano. Lett. 11: 5279-5283.

15. Afinogenov B I, Popkova A A, Bessonov V O, Fedyanin A A, (2016) Measurements of the femtosecond relaxation dynamics of Tamm plasmon-polaritons. Appl. Phys. Lett. 109: 2349.

16. Gazzano O, Vasconcellos S M de, Gauthron K, Symonds C, Bloch J, Voisin P, Bellessa J, Lemaitre A, Senellart P (2011) Full control of spontaneous emission in confined Tamm plasmon structures.

17. Zhang C, Wu K, Giannini V, Li X (2017) Planar Hot-Electron Photodetection with Tamm Plasmons. Acs. Nano. 11: 1719-1727.

18. Qing Y M, Ma H F, Cui T J (2019) Flexible control of light trapping and localization in a hybrid Tamm plasmonic system. Opt. Lett. 44: 3302.

19. Grigorenko A N, Polini M, and Novoselov K S (2012) Graphene plasmonics. Nature Photonics 6(11): 749-758.

20. Jablan M, Buljan H, and Soljacic M (2009) Plasmonics in graphene at infrared frequencies. Physical Review 80(24): 245435.1-245435.7.

21. Feng Y, Hu Z D, Wang J C, Balmakou A, Khakhomov S, Semchenko I, Liu D D, Sang T (2020) Perfect Narrowband Absorber based on Patterned Graphene-Silica Multilayer Hyperbolic Metamaterials. Plasmonics, 15(6): 1869 -1874.

22. Ju L, Geng B S, Horng J, Girit C, and Martin M (2011) Graphene plasmonics for tunable terahertz metamaterials. Nat. Nanotechnol 6(10): 630-634.

23. Ren Y, Guo X, Zhang G, Balakin A V, Shkurinov A P, Yu A, and Zhu Y (2020) Excitation of graphene surface plasmons polaritons by guided-mode resonances with high efficiency. Opt. Express 28: 13224-13233.

24. Wang J C, Yang L, Hu Z D, He W J, Zheng G G (2019) Analysis of graphene-based multilayer comb-like absorption enhancement system based on multiple waveguide theory. IEEE Photonics Technology Letters, 31(7): 561-564..

25. Hua L U, Gan X, Jia B, Mao D, Zhao A J (2016) Tunable high-efficiency light absorption of monolayer graphene via Tamm plasmon polaritons. Opt. Lett. 41: 4743-4746.

26. Cheng H C, Kuo C Y, Hung Y J, Chen K P, Jeng S C (2018) Liquid-Crystal Active Tamm-Plasmon Devices. Phys. Rev. Appl 9: 64034.

27. Matthias, Wurdack, Nils, Lundt, Martin, Klaas, Vasilij, Baumann, Alexey, and V (2017) Observation of hybrid Tamm-plasmon exciton-polaritons with GaAs quantum wells and a MoSe2 monolayer. Nat. Commun.

28. Mischok A, Siegmund B, Ghosh D S, Benduhn J, Spoltore D, Bhm M, Frb H, Koerner C, Leo K, Vandewal K (2017) Controlling Tamm Plasmons for Organic Narrowband Near-Infrared Photodetectors. Acs. Photonics. 7b00427.

29. Maji P S, Das R (2017) Hybrid-Tamm-Plasmon-Polariton Based Self-Reference Temperature Sensor. J Lightwave Technol 35: 2833-2839.

30.Kumar S, Shukla M K, Maji P S, Das R (2017) Self-referenced refractive index sensing with hybrid-Tamm-plasmon-polariton modes in sub-wavelength analyte layers. Journal of Physics D Applied Physics.

31.Zhou H, Yang G, Wang K, Long H, Lu P (2010) Multiple optical Tamm states at a metal – dielectric mirror interface. Opt. Lett. 35: 4112.

32.Hu J, Qing Y, Yang S, Ren Y, Wu X, Gao W, Wu C (2017) Tailoring total absorption in a graphene monolayer covered subwavelength multilayer dielectric grating structure at near-infrared frequencies. Journal of the Optical Society of America. B, Optical physics 34: 861.

33.Dao T D, Ishii S, Doan A T, Wada Y, Ohi A, Nabatame T, Nagao T (2019) An On-Chip Quad-Wavelength Pyroelectric Sensor for Spectroscopic Infrared Sensing. Adv. Sci. 6: 1900579.

34.Zheng H Y, Jin X R, Park J W, Lu Y H, Rhee J Y, Jang W H, Cheong H, Lee Y P (2012) Tunable dual-band perfect absorbers based on extraordinary optical transmission and Fabry-Perot cavity resonance. Opt. Express 20: 24002-24009.

35.Fu X Y, Yi K, Shao J D, Fan Z X (2009) Design of single-material guided-mode resonance filter. Chin. Opt. Lett. 7: 9-11.

36.Cai Y, Huang Y, Zhu K, Wu H (2019) Direction-independent dual-band perfect absorption induced by fundamental magnetic polaritons. Opt. Express 27: A1431.

37.Hu J, Yao E, Xie W, Liu W, Li D, Lu Y, Zhan Q (2019) Strong longitudinal coupling of Tamm plasmon polaritons in graphene/DBR/Ag hybrid structure. Opt. Express 27: 18642.

38.Zhang D, Qiu D, Chen Y, Wang R, Zhu L, Wang P, Ming H, Badugu R, Stella U, Descrovi E (2019) Coupling of Fluorophores in Single Nanoapertures with Tamm Plasmon Structures. J. Phys. Chem. C.

39.Nong J, Wei W, Wang W, Lan G, Shang Z, Yi J, Tang L (2018) Strong coherent coupling between graphene surface plasmons and anisotropic black phosphorus localized surface plasmons. Opt. Express 26: 1633.

40.Hu T,Wang Y, Wu L, Zhang L, Shan Y, Lu J, Wang J, Luo S, Zhang Z, Liao L (2007) Strong coupling between Tamm plasmon polariton and two dimensional semiconductor excitons. Appl. Phys. Lett. 110: 51101.

41.Wang J C, Wang X Y, Hu Z D, Tang Y, Balmakou A, Khakhomov S, Liu D (2019) Independent tunable multi-band absorbers based on molybdenum disulfide metasurfaces. Physical chemistry chemical physics: PCCP 21(43): 24132-24138.

42.Bao Z Y, Wang J C, Hu Z D, Balmakou A, Zhang C (2019) Coordinated multi-band angle insensitive selection absorber based on graphene metamaterials. Opt. Express 27: 31435.

43.Buzavaite-Verteliene E, Valavicius A, Grineviciute L, Tolenis T, Lukose, Niaura G, Balevicius Z (2020) Influence of the graphene layer on the strong coupling in the hybrid Tamm-plasmon polariton mode. Opt. Express 28: 10308-10319.

Figures

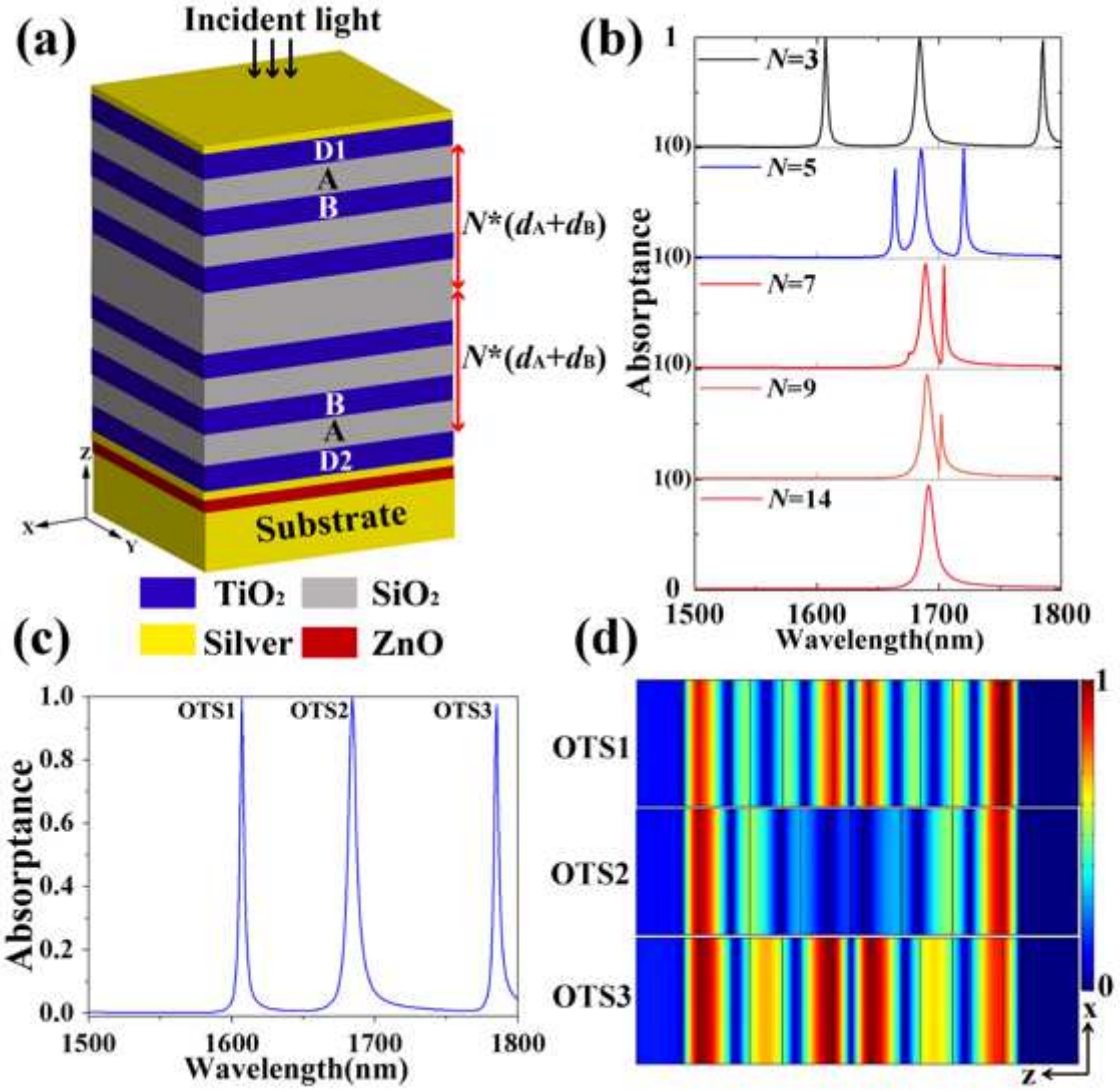

Figure 1

(a) Schematic diagram of the structure composed of upper silver film/PCH/lower silver film/ZnO/silver substrate; (b) The two side peaks can be eliminated by increasing the number of layers N of the dual PhCs; (c) The three perfect absorption peaks were realized for the depicted structure when N=3; (d) The electric field distributions for the three peaks corresponding to TPP modes: OTS1, OTS2, OTS3.

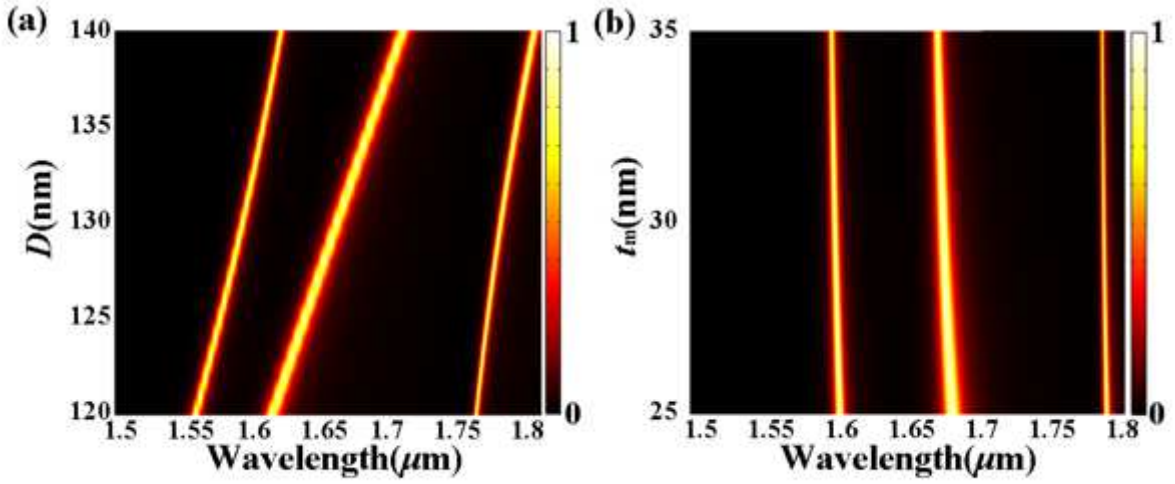

Figure 2

Spectral diagrams determine the absorptance peak positioning depending on: (a) the thickness D and (b) tm.

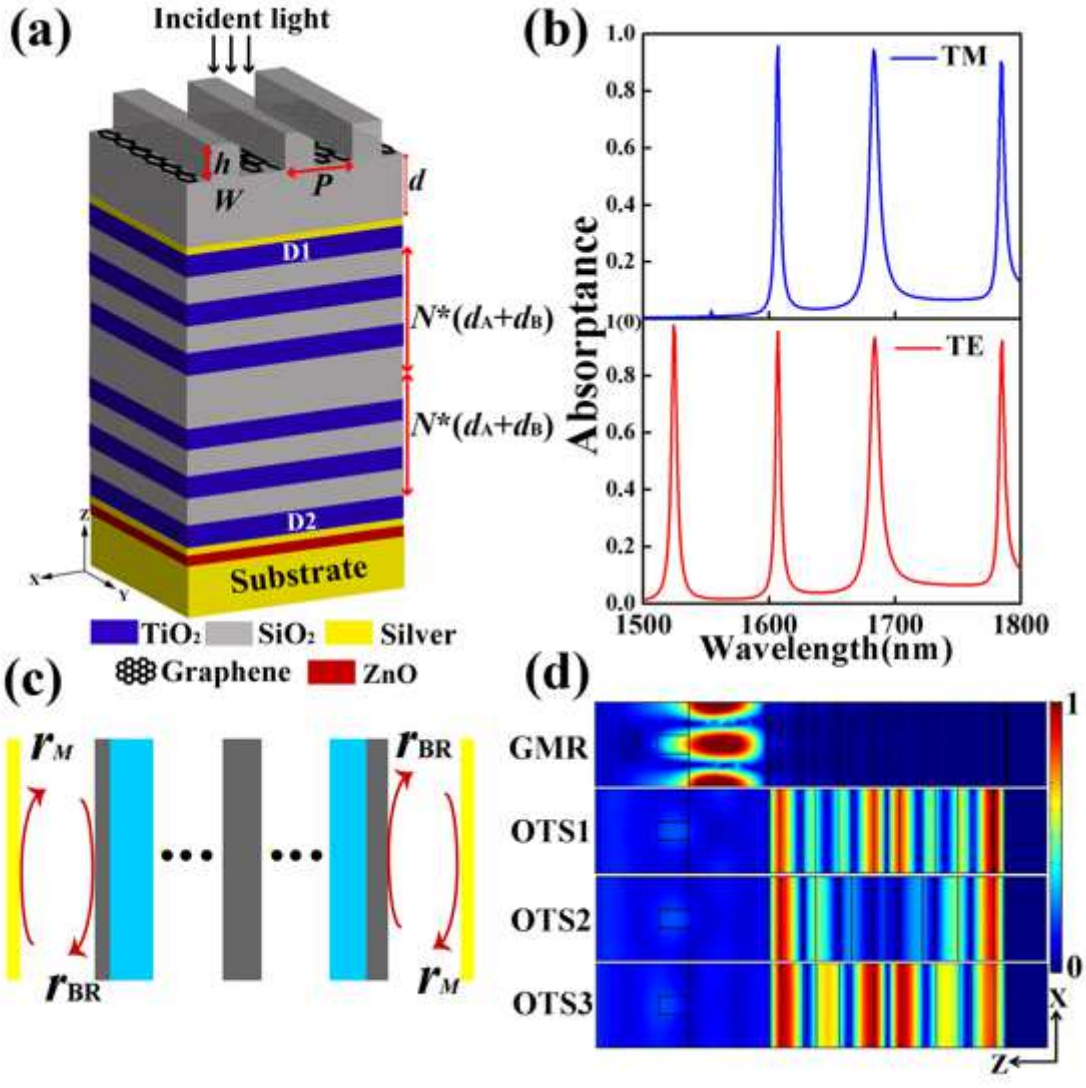

Figure 3

(a) Three-dimensional schema of the multichannel absorption filter; (b) Absorption spectra when incident with TM and TE polarization respectively; (c) shows two identical cavities, both wrapped by silver films and BRs; (d) Electric field magnitude for the GMR and for three TPP modes when incident with TE polarization.

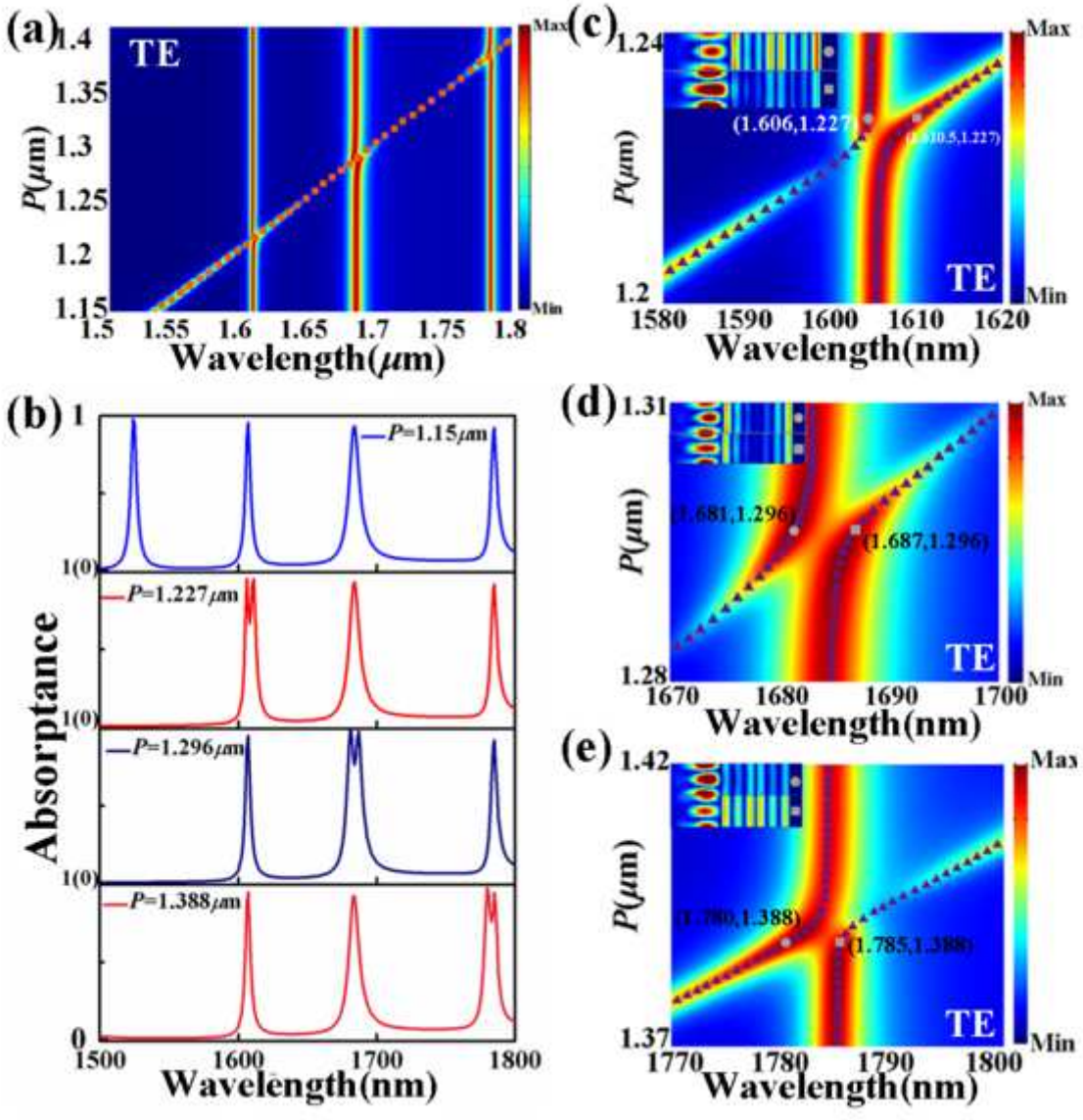

Figure 4

Evolution of absorption spectra of (a) the hybridized Tamm structure with the grating period length P, where the red square indicate the GMR; (b) Absorption spectrum at specific P; (c), (d), (e) are enlarged views of the absorption spectra at the three resonance coupling locationsare. The insets show the enhanced electric field resonance of GMR and TPP at the locations marked by hexagons and squares.

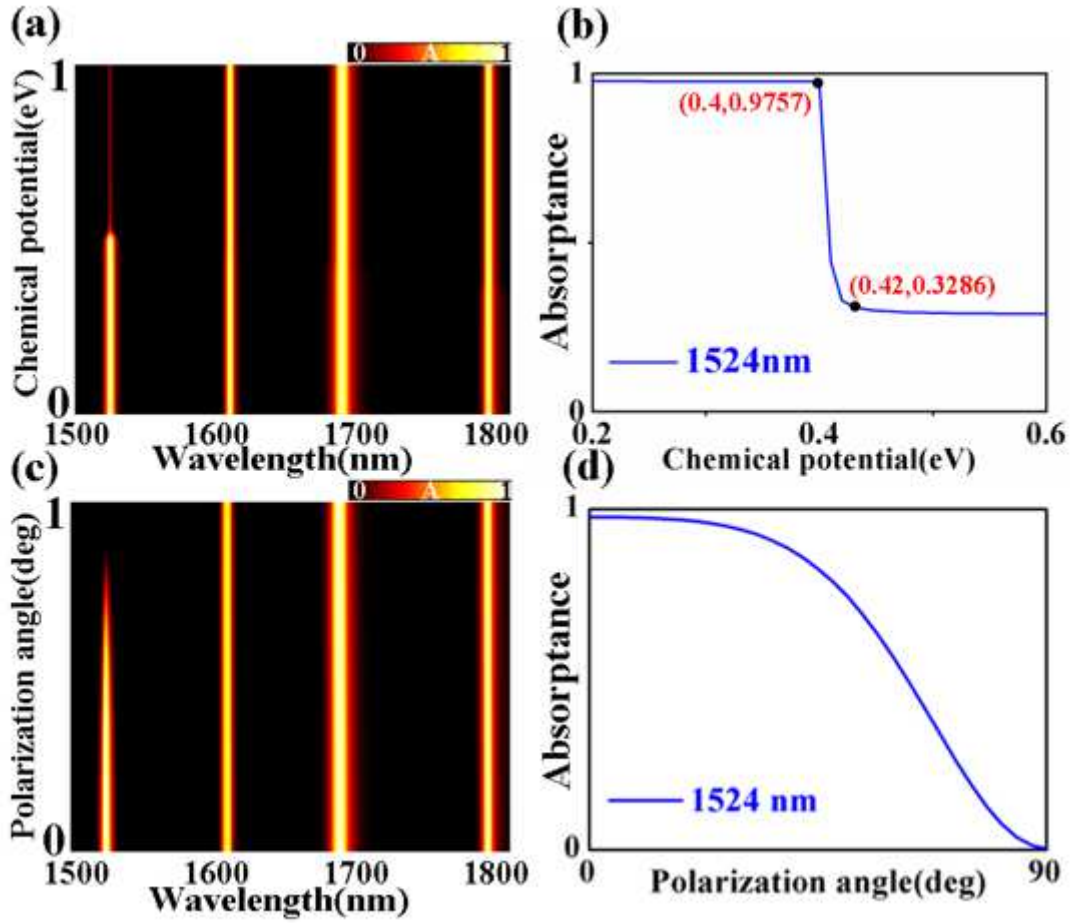

Figure 5

(a) Spectral diagram representing the dependence of the absorption as a function of the wavelength and the chemical potential of graphene under TE polarization. (b) The dependence of absorptance versus chemical potential at 1524 nm. (c) Spectral diagram representing the dependence of the absorptance as a function of the wavelength and the polarization angle at normal incidence. (d) The dependence of absorptance versus chemical potential at 1524 nm.